AGU PUBLICATIONS

JGR

Journal of Geophysical Research: Solid Earth

RESEARCH ARTICLE
10.1002/2014JB011403

Special Section:
Stress, Strain and Mass Changes at Volcanoes

Key Points:
- Intraplate volcanic provinces can be related to a slow creep damage
- Coupled damage feedback may explain volcanism in low heat flow settings
- Triple lithosphere damage may be important to plate tectonics

Correspondence to:
G. Rosenbaum,
g.rosenbaum@uq.edu.au

Citation:
Regenauer-Lieb, K., G. Rosenbaum, V. Lyakhovsky, J. Liu, R. Weinberg, A. Segev, and Y. Weinstein (2015), Melt instabilities in an intraplate lithosphere and implications for volcanism in the Harrat Ash-Shaam volcanic field (NW Arabia), *J. Geophys. Res. Solid Earth*, *120*, doi:10.1002/2014JB011403.

Received 26 JUN 2014
Accepted 19 FEB 2015
Accepted article online 24 FEB 2015

Melt instabilities in an intraplate lithosphere and implications for volcanism in the Harrat Ash-Shaam volcanic field (NW Arabia)

Klaus Regenauer-Lieb[1,2], Gideon Rosenbaum[3], Vladimir Lyakhovsky[4], Jie Liu[5], Roberto Weinberg[6], Amit Segev[4], and Yishai Weinstein[7]

[1]School of Petroleum Engineering, Tyree Energy Technologies Building, University of New South Wales, Sydney, New South Wales, Australia, [2]CSIRO Earth Science and Resource Engineering, Australian Resources Research Centre, Perth, Western Australia, Australia, [3]School of Earth Sciences, University of Queensland, Brisbane, Queensland, Australia, [4]Geological Survey of Israel, Jerusalem, Israel, [5]School of Earth Science and Geological Engineering, Supercomputing Institute, Sun Yat-sen University, Guangzhou, China, [6]School of Earth, Atmosphere, and Environment, Monash University, Clayton, Victoria, Australia, [7]Department of Geography and Environment, Bar-Ilan University, Ramat-Gan, Israel

Abstract We investigate melt generation in a slowly extending lithosphere with the aim of understanding the spatial and temporal relationships between magmatism and preexisting rift systems. We present numerical models that consider feedback between melt generation and lithospheric deformation, and we incorporate three different damage mechanisms: brittle damage, creep damage, and melt damage. Melt conditions are calculated with a Helmholtz free energy minimization method, and the energy equation is solved self-consistently for latent heat and shear heating effects. Using a case of a slowly extending (1–1.5 mm/yr) continental lithosphere with a relatively low surface heat flow (~50 mW/m^2), we show that melt-rich shear bands are nucleated at the bottom of the lithosphere as a result of shear heating and damage mechanisms. Upon further deformation, melt zones intersect creep damage zones, thus forming channels that may be used for the melt to migrate upward. If a preexisting structure resides only in the brittle crust, it does not control the path of melt migration to the surface, and melt-filled channels propagate from the bottom upwards, independently of upper crustal structures. In contrast, a preexisting weak structure that reaches a critical depth of 20 km allows fast (~2 Ma) propagation of melt-filled channels that link melt damage from the bottom of the lithosphere to near-surface structures. Our model results may explain the short time scale, volume, and magma extraction from the asthenosphere through a low surface heat flow lithosphere, such as observed, for example, in the Harrat Ash-Shaam volcanic field (northwestern Arabia), which developed in the Arabian Plate and is spatially linked to the Azraq-Sirhan Graben.

1. Introduction

Intraplate volcanism is a ubiquitous phenomenon attributed to a variety of mechanisms, such as plume-lithosphere interaction [*Anderson et al*., 1992; *Eldholm and Grue*, 1994; *Willan and Kelley*, 1999], asthenospheric shear [*Conrad et al*., 2011], and lithospheric extension [*Wilson and Downes*, 1992]. Cenozoic intraplate volcanism in Europe, for example, was associated with rifting and has been maintained even though extension rates were extremely slow (1–2 mm/yr) [*Regenauer-Lieb and Petit*, 1997; *Nocquet et al*., 2001]. Strongly deformed mantle xenoliths from this rift system are characterized by mantle metasomatism, showing geochemical enrichment processes associated with melting and shearing [*Downes*, 1990]. This indicates that the passage of melt has been associated with an intricate link between a slowly deformed lithosphere, high degree of localization, and fluid alteration.

Another example where melting was generated and maintained in an intraplate environment is the melt production associated with the Harrat Ash-Shaam volcanic field, which has generated melts for the last ~30 Ma in the proximity of the Azraq-Sirhan Graben (Figure 1) [*Segev et al*., 2011, 2014]. This graben, which is about 40 km wide and 700 km long, is located on the northwestern edge of the Arabian continent (Figure 1a). The initial stage of rifting occurred in the Late Cretaceous without volcanic activity and prior to the onset of magmatism volcanism in the northeastern Afro-Arabia plate at ~30 Ma [*Avni et al*., 2012]. Some of these structures were reactivated during the Oligocene-Miocene extension of the Arabian Plate, which was accommodated along the Suez/Red Sea rift [*Steckler and ten Brink*, 1986] and, to a lesser extent,

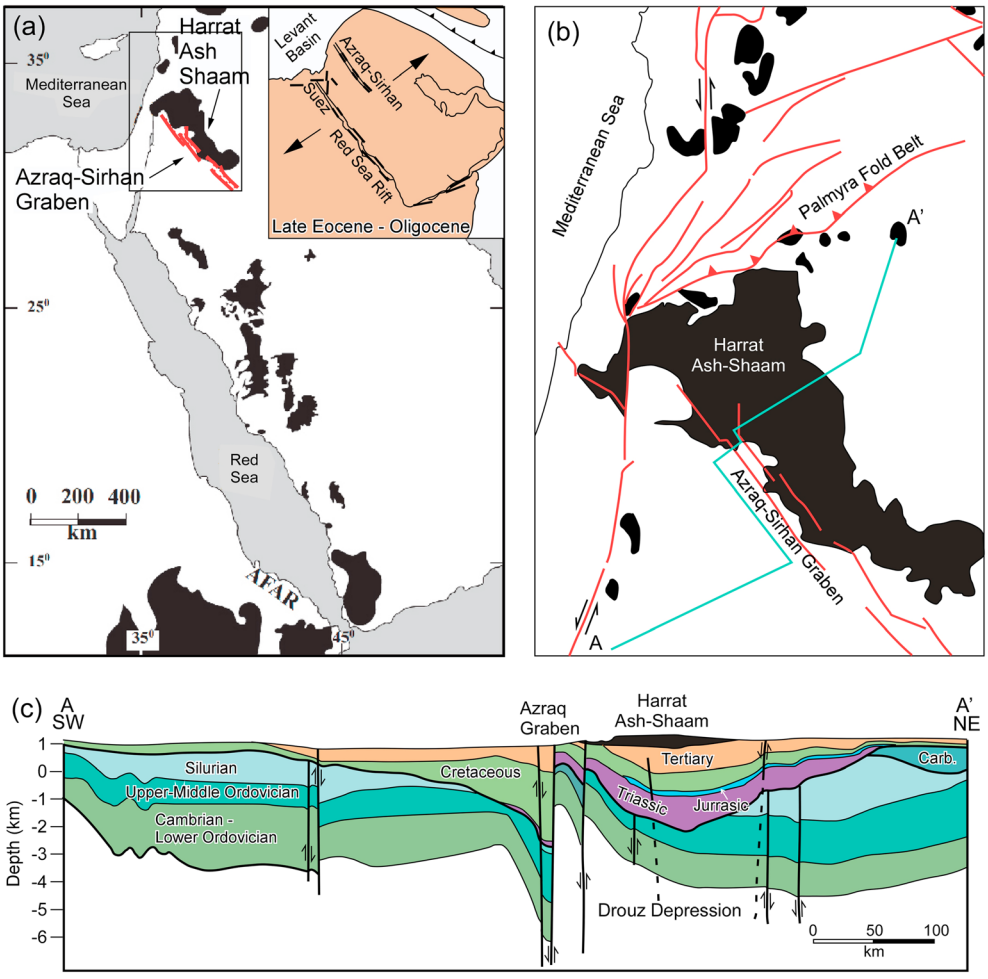

Figure 1. (a) Location map of the Harrat Ash-Shaam volcanic field and Azraq-Sirhan Graben and the distribution of Cenozoic volcanism (black areas) in the western Arabian Peninsula [after *Weinstein et al.*, 2006]. The inset shows a schematic reconstruction of Arabia during the late Eocene to Oligocene [after *Segev et al.*, 2014]. (b) Tectonic map of the northwestern Arabian Plate [after *Segev et al.*, 2011]. (c) Cross section across the Azraq-Sirhan Graben [after *Konert et al.*, 2001].

in the Azraq-Sirhan Graben [*Sharland et al.*, 2001; *Schattner et al.*, 2006; *Segev and Rybakov*, 2010, 2011]. Both rifts propagated during the Oligocene toward the northwest and terminated at the Levant continental margin (Figure 1a). Cenozoic extension in the Azraq-Sirhan Graben was relatively minor, and the deformation rates are assumed to be low. Nevertheless, in spite of the low extension, the existence of this rift system has apparently played a role in localizing post Oligocene (<30 Ma) magmatism [*Segev et al.*, 2011, 2014].

The mafic volcanic field of Harrat Ash-Shaam, which is located along the margin of the Azraq-Sirhan Graben (Figure 1b), is associated with Oligocene to recent volcanism. The maximum melt thickness (Figure 1c) exceeds 1 km both at the Drouz Depression [*Razvalyaev et al.*, 2005; *Meiler et al.*, 2011; *Segev et al.*, 2014] and near the Sea of Galilee [e.g., *Garfunkel*, 1989]. Based on modern heat flow data [*Shalev et al.*, 2013, and references therein] and the thermal history of the Levant area [e.g., *Segev et al.*, 2014], the larger area comprising the Arabian Shield is characterized by low heat flow, probably below ~50 mW/m^2 (with the exception of the areas next to the Dead Sea rift valley [*Förster et al.*, 2007, 2010; *Shalev et al.*, 2013]). How exactly melting has been maintained within such a low heat flow environment and inferred slowly deforming lithosphere [e.g., *Segev et al.*, 2014], and the reason why melt of the Harrat Ash-Shaam volcanic field is localized in the proximity of the Azraq-Sirhan Graben, remains a puzzle. Some authors attributed the melting to the emplacement of an anomalously hot mantle beneath this area [e.g., *Garfunkel*, 1989;

Camp et al., 1992; *Weinstein et al*., 2006; *Ma et al*., 2011], but the current low heat flow in the area makes it an unlikely scenario.

In this paper, we provide an alternative explanation to the origin of melt in an intracontinental setting with assumed slow deformation rates and low heat flow. We explore explicitly the origin of melt by means of numerical modeling that considers a number of damage mechanisms as a result of mechanical deformation [*Liu et al*., 2014]. The consideration of brittle damage, ductile damage, and melt damage in our numerical formulation is shown to be capable of generating local, low-volume lithospheric melting within shear zones. Although we do not model melt propagation, we assume that the melt may propagate upward and link with fault zones in the upper crust, thus explaining melt transfer in the proximity of slowly deforming rift zones, such as the Azraq-Sirhan Graben and the central European rift system. We emphasize, however, that our models are designed to explore the fundamental behavior of a slowly extending continental lithosphere and are not meant to make predictions on the particular geological processes occurring in the lithosphere. The models' inputs (e.g., extension rates and heat flow) are speculative, and the models are aimed at developing a scenario that is consistent with the geological and rheological assumptions.

2. Modeling Approach

2.1. Coupled Brittle, Creep, and Melt Damage

We have incorporated in our calculations three important micromechanisms that generate microporosity, and we assess their effect on the overall behavior of the lithosphere. The first mechanism is associated with brittle fracturing triggered, for example, by seismic events. The second mechanism is associated with longer time scale creep processes, which is expected to occur above a critical temperature for thermal activation of a particular diagenetic or metamorphic mineral breakdown reaction (e.g., dissolution-precipitation creep of *K* feldspar at midcrustal conditions [*Menegon et al*., 2008]). The third mechanism is the melt generation on grain boundary triple junctions.

Explicit simulations of such microcracks and voids require temporal upscaling from milliseconds to millions of years and spatial upscaling from micrometers to hundreds of kilometers. However, this is presently impossible to achieve. We therefore use a simplification, in which an implicit description of the microporosity generation processes is provided by integration over several cycles. The approach is known as a smeared crack, or damage mechanics approach, and it means that rather than modeling each individual microcrack, an assembly of microcracks is integrated over time and space. The overall effect of these microcracks on the mechanical behavior of a representative volume element (REV) is assessed [*Regenauer-Lieb et al*., 2013a, 2013b]. The long time scale behavior of the REV is subsequently modeled using a thermodynamic evolution law based on the sum of the individual microporosity generating mechanisms and an implicit time integration scheme.

The thermodynamic evolution relies on three key feedback (Figure 2), which are based on the consideration of brittle, creep, and melt damage. The brittle damage mechanism is elastoplastic and stems from dilational deformation that weakens the strength of rocks by generating high-porosity shear bands [*Karrech et al*., 2011b]. A similar mechanism has been postulated to operate also in the ductile regime in the presence of metamorphic fluids or melts, giving rise to fluid or melt-filled creep/ductile fractures, similar to the dilational fractures in the brittle regime [*Regenauer-Lieb*, 1999; *Weinberg and Regenauer-Lieb*, 2010].

The metamorphic fluid and melt damage mechanisms require that viscous creep accumulates and aligns fluids on grain boundaries. This mechanism is well known in material sciences [*Ghandi and Ashby*, 1979]. Early experiments with rock analogues clearly showed the importance of this mechanism for geological processes [*Raj*, 1982]. Creep/ductile fractures have been incorporated in numerical modeling of the lithosphere [*Regenauer-Lieb*, 1999], and their existence was further supported by controlled laboratory experiments [*Rybacki et al*., 2008] and synchrotron X-ray-computed tomography analyses on naturally deformed samples at upper greenschist facies conditions [*Fusseis et al*., 2009]. Furthermore, geological field observations describe fluid-phase-assisted opening of micropores through creep in rock specimens that have been deformed in a ductile manner mostly at midcrustal conditions [*Fliertvoet et al*., 1997; *Eichhubl and Aydin*, 2002; *Menegon et al*., 2008]. A summary of the material science background, the experimental verification, and the geological implications can be found in *Rybacki et al*. [2010].

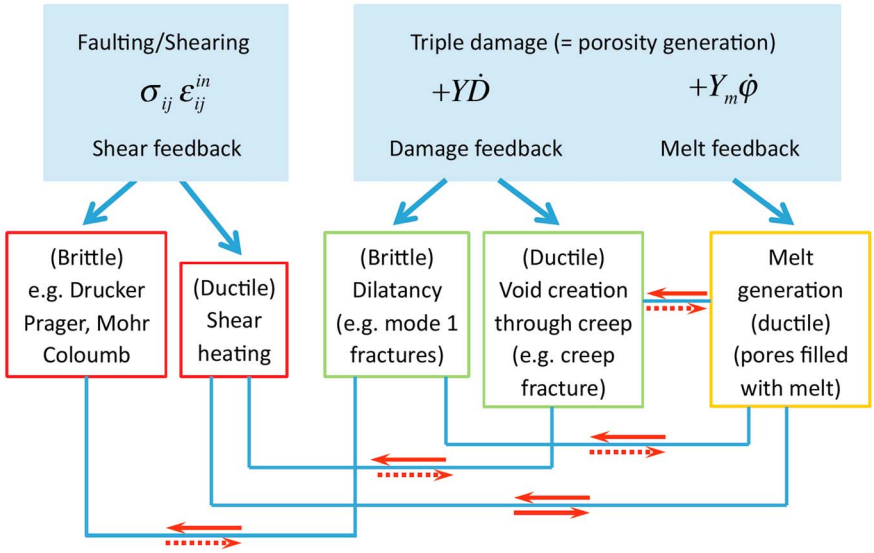

Figure 2. Schematic illustration of the various feedback mechanisms and their possible interactions as well as their equivalence in classical mechanical formulations that are not derived from energy considerations.

Creep/ductile fractures are modeled here in conjunction and competition with classical brittle fractures. We follow a continuum mechanics approach that considers the energy equation (thermodynamic constraints) in addition to the continuity of mass and momentum. In geomechanical modeling, the energy equation is not explicitly coupled to the equilibrium of mass and momentum, so our approach offers a higher order (energy) perspective of geological processes.

In order to allow energy-based modeling, we choose a thermodynamic potential as a common energetic reference frame. In chemical modeling, it is often convenient to choose a Gibbs free energy framework. Gibbs free energy is the total energy that is needed to create a chemical system and make room for it, minus the energy received from the environment. In mechanical deformation, the volumetric deformation is considered explicitly, and the use of the partial Legendre transform of the Gibbs free energy is preferred. This leads to the use of the Helmholtz free energy, where the deformational energy that is required to make room for the system is implicitly considered. A Helmholtz free energy deformation theory for coupled brittle/ductile damage has been presented in *Karrech et al*. [2011a]. Melt damage is incorporated by including latent heat effects for specific Helmholtz free energy ψ:

$$\begin{aligned}\rho\psi\left(\epsilon_{ij},\epsilon_{ij}^{in},T,D,\varphi_m\right) &= (1-D)G\varphi_m\epsilon_{ij}^{e}+\frac{1}{2}\left[(1-\varphi_m)(1-D)\lambda^{e}+\varphi_m\lambda_m^{e}\right]\left(\epsilon_{ij}^{e}\right)^2\\ &-3\left[(1-\varphi_m)(1-D)K\alpha+\varphi_m K_m\alpha_m\right]\epsilon_{kk}^{e}(T-T_0)\\ &-\left[(1-\varphi_m)c+\varphi_m c_m\right]\frac{(T-T_0)^2}{2T_0}+L\varphi_m\end{aligned} \tag{1}$$

where ρ is the material density; ϵ_{ij} is the total strain tensor; ϵ_{ij}^{in} is the inelastic strain tensor and $\epsilon_{ij}^{e}=\epsilon_{ij}-\epsilon_{ij}^{in}$ is the elastic strain tensor; T is the temperature and T_0 is a reference temperature; D is the mechanical damage parameter of solid part; φ_m is the melt fraction by volume; G is the shear modulus of solid; λ^{e} and λ_m^{e} are the first Lame's constant of solid and melt, respectively; K and K_m are bulk modulus for solid and melt; α and α_m are the coefficient of thermal expansion of solid and melt; and c and c_m are the specific heat capacity of solid and melt, respectively. The nonlinear temperature term accounts for the variation of heat capacity with temperature [*Houlsby and Puzrin*, 2007], while the last term describes the important energetic effect of melting related to the latent heat L. Since we do not solve the equations for melt transfer in our damage mechanical solver, we limit the melt fraction φ_m to 20%, which is much lower than the other damage mechanisms. This underestimates the weakening for large melt fraction but is acceptable for small fraction. Thus, we present a conservative estimate of the mechanical effects of the melt generation.

The derivative of Helmholtz specific free energy with respect to time t is

$$\rho\frac{\partial\psi}{\partial t}=\rho\frac{\partial\psi}{\partial\epsilon^e_{ij}}\,\dot{\epsilon}^e_{ij}+\rho\frac{\partial\psi}{\partial T}\,\dot{T}+\rho\frac{\partial\psi}{\partial D}\,\dot{D}+\rho\frac{\partial\psi}{\partial\phi_m}\dot{\phi}_m \tag{2}$$

Using the first and second laws of thermodynamics, we obtain

$$\begin{aligned}\rho\frac{\partial\psi}{\partial\epsilon^e_{ij}}=\sigma_{ij}=2(1-D)Ge^e_{ij}+\left[(1-\varphi_m)(1-D)\lambda^e+\varphi_m\lambda^e_m\right]\epsilon^e_{ii}\delta_{ij}\\+3\left[(1-\varphi_m)(1-D)K\alpha+\varphi_m K_m\lambda_m\right](T-T_0)\delta_{ij}\end{aligned} \tag{3}$$

$$\rho\frac{\partial\psi}{\partial D}=Y_D=-G\epsilon^e_{ij}\epsilon^e_{ij}-\frac{1}{2}(1-\varphi_m)\lambda^e\left(\epsilon^e_{ii}\right)^2+3(1-\varphi_m)K\alpha\epsilon^e_{ii} \tag{4}$$

$$\rho\frac{\partial\psi}{\partial\varphi_m}=Y_m=-\frac{1}{2}\left[\lambda^e_m-(1-D)\lambda^e\right]\left(\epsilon^e_{kk}\right)^2-3\left[K_m\alpha_m-(1-D)K\alpha\right](T-T_0)\epsilon^e_{kk}-(c-c_m)\frac{(T-T_0)^2}{2T_0}+L \tag{5}$$

The volume strain ϵ^e_{kk} can be expressed by the deformed and undeformed volumes. Thus, equation (5) can be written as

$$Y_m=\frac{1}{2}\left[\lambda^e_m-(1-D)\lambda^e\right]\left(\frac{V-V_0}{V_0}\right)^2-3\left[K_m\alpha_m-(1-D)K\alpha\right](T-T_0)\left(\frac{V-V_0}{V_0}\right)-(c-c_m)\frac{(T-T_0)^2}{2T_0}+L \tag{6}$$

The enriched continuum formulation [*Karrech et al*., 2011a] is an extension of a thermodynamic approach [*Regenauer-Lieb and Yuen*, 2003] where the intrinsic dissipation function (rate of energy dissipated through the product of a thermodynamic force times a thermodynamic flux) is composed of three potential localization mechanisms:

$$(1-\chi)Di=Di_1+Di_2+Di_3$$

where χ is known as the Taylor-Quinney coefficient, which describes the efficiency of converting mechanical work into heat, and $(1-\chi)Di$ is the total mechanical work that is not dissipated into heat during deformation. For the selection of a parameter value, we rely on thermographic experiments performed for a variety of materials, which show a surprisingly common value for χ. For example, experiments by *Chrysochoos and Belmahjoub* [1992] showed that χ is quickly increased to a steady state value of 0.9–0.8. Our calculations are based on steady state flow laws, and therefore, a value of $\chi=0.9$ is used.

For simplicity, we only discuss here the portion of mechanical work that is transferred into damage. This damage has three forms. Di_1 encompasses the classical brittle deformation through an elastoplastic damage mechanics approach. Note that in the enriched thermodynamic continuum framework, this mechanism integrates over long geological time scales equivalent to several earthquake cycles with a periodic quasi-steady state. The damage parameter is a measure for effective pore space that weakens the rock matrix. In geological terms, this corresponds to the weakening effect of the brittle fault valve process averaged over several cycles [*Sibson*, 1985].

Di_2 describes the equivalent process formulating a quasi steady state weakening process in the ductile regime [*Poulet et al*., 2014; *Veveakis and Poulet*, 2014]. The damage mechanism is a creep damage/fracture, and the damage parameter quantifies the integrated effective weakening of the rock matrix from an energy perspective, assuming an oscillatory steady state.

Di_3 is the melt damage mechanism, formally equivalent to the melt fraction. This is the simplest damage mechanism that does not require postulating a quasi-steady state. In the energy consideration, it follows

simply from the Helmholtz free energy minimization, assuming local thermodynamic equilibrium to calculate when melting occurs.

In terms of energy quantities, the damage processes are related to the product of the stress (thermodynamic force) times the inelastic strain rate (thermodynamic flux):

$$Di = \sigma_{ij}\dot{\varepsilon}_{ij}^{in}$$

This is equivalent to the total rate of mechanical work dissipated in the deforming body.

The brittle/creep damage term is the mechanical damage feedback (Figure 2):

$$Di_{1,2} = Y\,\dot{D}$$

where $\dot{D}$ is the rate of change of the mechanical damage parameter (the thermodynamic flux) and Y is the associated thermodynamic force. This can be derived from the partial derivative of the Helmholtz free energy over the damage parameter [*Karrech et al*., 2011a]. Two fundamentally different processes are considered. The first process (D_1) may be interpreted as brittle dilatancy, while the second process (D_2) is a creep damage caused by the slow creep deformation of the solid rock matrix and the associated growth/shrinkage of micropores. An important assumption that is required for this mechanism to occur is that fluid is available to fill the brittle or ductile fracture. This fluid can be meteoric (in the brittle zone), metamorphic through dehydration reactions or a fluid flux from below (in the ductile zone), or a melt source.

The third term is the melt damage (Figure 2):

$$Di_3 = Y_m\dot{\varphi}_m$$

where φ_m is the melt fraction by volume (melt porosity and its time derivative is the thermodynamic flux) and Y_m is the associated thermodynamic force, which can be derived from the partial derivative of the Helmholtz free energy over the melt fraction [*Liu et al*., 2014].

We propose that the problem of intraplate volcanism in a low heat flow lithosphere can be solved by this melt-assisted damage formulation, which is capable of describing (a) the thermodynamic condition for melting, (b) the expected partial melt distribution, (c) the feedback between melt formation and ductile deformation, and (d) the link to the shallower ductile and brittle instabilities. The model has no favorite damage mechanism, and it selects the appropriate damage mode according to the local energetic condition. This means that brittle damage is possible at any depth if the stresses are high enough, and melt-assisted shear bands can propagate upward to any depth if the thermodynamic conditions allow melting at shallower depths.

2.2. Modeling Melt Damage (Di_3)

We first define the time scale of integration of the melt fraction. In order to calculate the percentage of partial melt and the melt composition, we select a time scale that is sufficiently long to allow thermodynamic equilibrium of the chemistry in the considered REV. We can then calculate the thermodynamic properties of the melts from an assumed initial chemical composition of the mantle underneath the Azraq-Sirhan Graben. For the sake of simplicity, we assume that generated melts have a mid-ocean ridge basalt (MORB) composition [*McKenzie and Onions*, 1991]. The melt composition is calculated from the MELTS series thermodynamic solvers (http://melts.ofm-research.org/index.html). The choice of MORB composition has been made for a first-order analysis to assess the effect of melt generation using the well studied MORB system. It provides a first-order determination of the depth where melting occurs, which is parameterized in our models by varying the mantle heat flow. A more detailed comparison to other melting models, such as alkali-basaltic composition, is beyond the scope of this paper.

The MELTS series solver is the most widely used platform for thermodynamic calculations in igneous systems. It is designed to facilitate thermodynamic modeling of phase equilibrium in magmatic systems. The MELTS series solver calculates the phase equilibrium of a given chemical system and determines whether, under the given thermodynamic condition the host rock is a solid, a solid that contains a melt fraction or a melt. This allows a self-consistent assessment of typical geodynamic scenarios leading to magmatic processes,

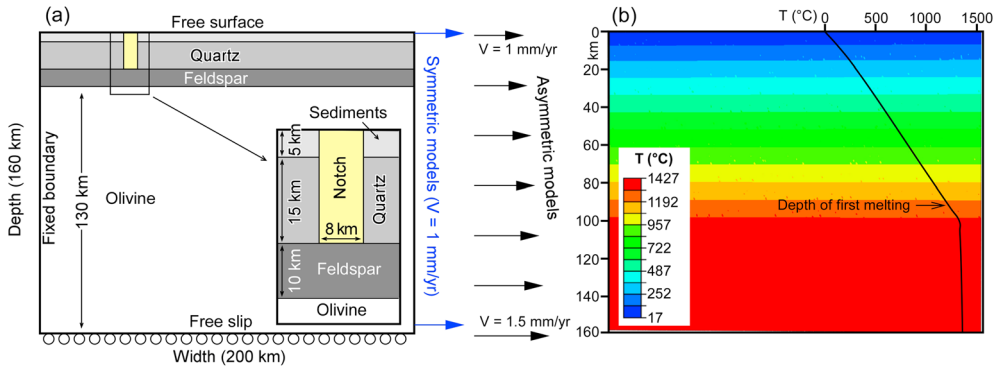

Figure 3. (a) Model setup showing four rheological layers and a notch. The blue arrows represent the extension velocity (V) in the symmetric models, and the black arrows represent the extension velocity in the asymmetric models. (b) Initial temperature field.

such as energy-constrained assimilation, adiabatic decompression melting, or equilibrium and fractional crystallization of magmas along a specified oxygen buffer.

The integration of the MELTS thermodynamic solver into a thermodynamically based geodynamic simulation opens new ways to numerically investigate melt generation processes. We emphasize that it is, however, important to solve the fully coupled energy balance during deformation and melting using a consistent energy framework. The damage mechanics approach [*Liu et al*., 2014] uses a Helmholtz free energy formulation, which is fully compatible with the Helmholtz free energy chemical solver of the MELTS thermodynamic suite. It allows thus for the first time to directly simulate numerically specific geological melt generation scenarios, such as melt generated by upwelling of the asthenosphere, the emplacement of an anomalously hot mantle, and the presence of a mantle lithosphere enriched in fusible minerals.

Output of the MELTS solver were incorporated as input into the implicit finite element solver Abaqus [*ABAQUS/Standard*, 2000] via a parameterization of the resulting melt fraction for different temperatures and pressures [*Liu et al*., 2014]. In other words, *P-T* at each point, resulting from the input of mechanical work into the shear zone and its resulting brittle and ductile damage, are assumed to be in equilibrium with the melt fraction. The properties obtained from the equilibrium melt calculations include parameters, such as density, viscosity, specific heat, entropy, and enthalpy. The most important parameter is the melt volume fraction, as this acts like an effective damage mechanism for the rock matrix similar to the classical damage mechanics approach [*Karrech et al*., 2011a]. Since we do not solve the equations for melt transfer in our damage mechanics solver, we limit the matrix weakening owing to partial melting to an arbitrary value of 20% melt. By doing so, we limit the mechanical role of melting instabilities. Although we do not model melt migration, we assume that, at this value, melt pathways are fully established and the percolation threshold is breached. In contrast to the melt damage, the brittle and ductile creep damage mechanisms can reach values up to 100%.

For the purpose of calculating the effect of melting on the damage of solid rock matrix, we extend a User Material Subroutine (UMAT) for Abaqus using the approach laid out by *Karrech et al*. [2011a, 2011b] in their previous work on creep and brittle damage. Technical details on the extension of the UMAT for inclusion of melt damage are presented elsewhere [*Liu et al*., 2014]. Melt damage can, in essence, be understood as a weakening effect of the solid rock matrix owing to the presence of melt. It is similar to the above described creep fracture where the melt phase replaces the metamorphic fluid. Note that in our formulation, we do not model melt flow and underestimate the weakening effect of melt on rock strength [*Holtzman et al*., 2012].

2.3. Model Setup

The model used is a variance of a simple model setup for a continental lithosphere under extension, which is described in detail elsewhere [*Regenauer-Lieb et al*., 2006; *Rosenbaum et al*., 2010]. The model assumes a horizontally stratified rheology consisting of the following layers (from top to bottom): (1) a 20 km thick quartz-rheology layer, including the top 5 km thick sedimentary layer that essentially behaves in a brittle manner; (2) a 10 km thick feldspar-rheology layer; and (3) a 130 km thick olivine-rheology layer (Figure 3a).

We do not model the formation of the Azraq-Sirhan Graben itself, which had supposedly developed in an earlier tectonic regime. Instead, we parameterize it by a deeply incised and sharply focused notch with variable depths

in the brittle crust. This starting model is a first-order approximation of the numerical simulations presented by *Lyakhovsky et al.* [2012], which demonstrate that gradual weakening and healing of the brittle rocks during early extension allow rifting under moderate tectonic stresses, without notable thinning of the lithosphere. It provides a feasible mechanism for the initial formation of a sharply incised localized graben, such as the Azraq-Sirhan. The results of *Lyakhovsky et al.* [2012] explain several geological observations but do not deal with the explicit modeling of the role of melting in the initial stages of rifting. Their calculations show, however, that a brittle rupture of the entire lithosphere [*Buck*, 2006] is unlikely to occur because the lower part of the lithosphere reacts in a dominantly ductile manner and cannot break at low applied stresses. Only the top surface can damage in a brittle manner, and there is no pathway for melts to the surface. The problem of deformation of the deeper architecture in the lithosphere, and the explicit role of lithosphere damage by melt generation, is the subject of the present contribution.

The vertical notch in our models is located 46 km from the left side and cuts the top layers (Figure 3a). In order to represent the effect of the deformation history of the preexisting Azraq-Sirhan Graben structure, we assigned an initial Young's modulus of the heavily fractured material in the notch to be 1 order of magnitude lower than the adjacent rocks. The notch is taken as an idealization of any perturbation in the lithosphere strength resulting from previous extension and formation of the localized brittle damage zone up to ~20 km depth [e.g., *Lyakhovsky et al.*, 2012]. It is used as a placeholder for any kind of material, thermal, or structural defects. This is justified based on the principle of Saint-Venant, whereby the difference between the effects of two different local perturbations becomes very small at sufficiently large distances from the perturbation. Consequently, the local width of the notch is not important and assumed to be constant (8 km), but its depth varies from one model to the other demonstrating sensitivity of the model results to the initial conditions. The rationale for varying its depth is to assess the possible thermal and structural perturbation from a previous rifting event, which is assumed to relax faster for higher temperatures and therefore implying a shallower notch depth.

The top boundary of the model is a free surface, while the bottom boundary is free slip in the *x* direction and pinned in the *y* direction. Both symmetric and asymmetric boundary conditions have been considered. Cenozoic extension was relatively minor, implying that extension rates were very low [*Segev et al.*, 2014, 2011]. Since no exact models for extension rates are available, we use a range of rates determined for extremely slow (1–2 mm/yr) intraplate extension [*Regenauer-Lieb and Petit*, 1997; *Nocquet et al.*, 2001].

Two different types of velocity boundary conditions are chosen. In the symmetric model, a total of 1 mm/yr extension was applied to the right side of the model. By holding the left side of the model fixed in *x* direction, the velocity boundary conditions are equivalent to symmetric extension of 0.5 mm/yr applied to both sides of the model. For the asymmetric case, we linearly increased the velocity at the right side of the model from 1 mm/yr at the top to 1.5 mm/yr at the bottom (Figure 3a). By smoothly varying the magnitude of the asymmetric component of the function, we can assess the transition from symmetric to asymmetric extension modes and the effect of asthenospheric shear [e.g., *Conrad et al.*, 2011].

The total size of the 2-D plane-strain model is 200 km wide and 160 km deep. The model was meshed to 392×196 rectangular elements. The initial element size is 510 m width and 816 m depth. This was chosen such that the elements on average will assume a perfect square shape at the end of the calculation, thus minimizing numerical errors and the need for remeshing.

The model parameters are summarized in Table 1. Further information on the model rheology and parameters are available in *Regenauer-Lieb et al.* [2006] and *Rosenbaum et al.* [2010]. Additional information on the damage rheology is described in *Karrech et al.* [2011a, 2011b].

2.4. Initial Thermal Gradient

We consider a basic thermal model controlled by the following ingredients. The heat flow at the bottom of the lithosphere is assumed to be 20–30 mW/m^2, while the crustal radiogenic heat production provides an additional contribution of 30–20 mW/m^2, such that the total surface heat flow equates to 50 mW/m^2 [*Turcotte and Schubert*, 2002]. Note that in the analytical model, the heat production is assumed to decay exponentially in the top 10 km of the upper crust, and we assume no heat production in the lower crust and mantle. The mantle value of 20–30 mW/m^2 therefore is a heat supply value to the base of the lithosphere from below and is not produced within the lithosphere itself.

Table 1. Parameters Used in the Numerical Model

Parameter	Name	Value	Units
χ	Shear heating efficiency	0.9	-
κ	Thermal conductivity	Quartz = 2.5 Feldspar = 2.5 Olivine = 3.2	W/(m · K)
α_{th}	Thermal expansion	3.1×10^{-5}	K^{-1}
c_p	Specific heat	4.0×10^{5}	J/(kg * K)
ρ	Density	Quartz = 2700 Feldspar = 2800 Olivine = 3300	kg/m^3
v	Poisson ratio	0.38	-
E	Young's modulus	4.5×10^{10}	Pa
A	Material constant-preexponential parameter	Quartz = 3.98×10^{-21} Feldspar = 7.94×10^{-26} Olivine = 6.31×10^{-12}	$Pa^{-n} s^{-1}$
n	Power-law exponent	Quartz = 2.6 Feldspar = 3.1 Olivine = 4.0	-
H	Activation enthalpy	Quartz = 134.0×10^3 Feldspar = 163.0×10^3 Olivine = 135.0×10^3	J/mol
B	Thickness of the radiogenic layer (top of crust)	10	km
Qs	Surface heat flow	50	mW/m^2
Q_m	Mantle heat flow	20–30	mW/m^2

The following values have been adopted for the base of the lithosphere:

$$T = 1600\ \mathrm{K}; \alpha = 3 \times 10^{-5}\ \mathrm{K}^{-1};\ c_p = 880\,\mathrm{Jkg}^{-1};\ g = 9.8\,\mathrm{m}^2\mathrm{s}^{-1}$$

The temperature gradient in the deeper mantle is chosen as the mantle adiabat $dT/dz = T\alpha g/c_p$ [*McKenzie and Bickle*, 1988]. We therefore obtain, at the bottom of the lithosphere, an adiabatic gradient of ~0.54°C/km. For the sake of simplicity, the bottom of the lithosphere is defined as a thermal boundary layer below a particular temperature. This temperature is given by the intersection of the steady state geotherm and the mantle adiabat. Consequently, the depth and actual temperature of this intersection point varies according to the different thermal models following their assumed mantle potential temperature of 1600 K, which defines the value of the adiabat at the Earth's surface. With this simple formulation, we suppress any additional convective instabilities at the base of the lithosphere, which are expected to take place on longer time scales than considered in the model.

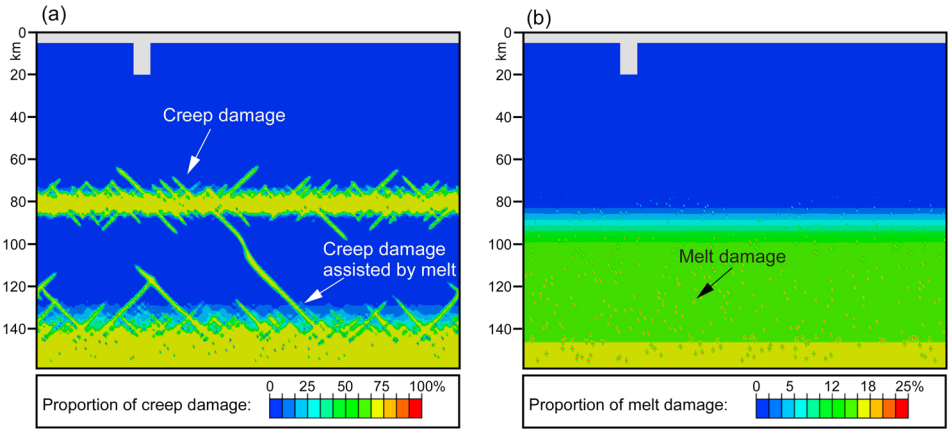

Figure 4. Comparison between (a) creep damage and (b) melt damage at time = 55 kyr in a model with a subcritical notch depth of 20 km, an asymmetric extension velocity, and a mantle heat flow of 30 mW/m^2. The legends refer to the respective proportion of damaged material in % of the REV.

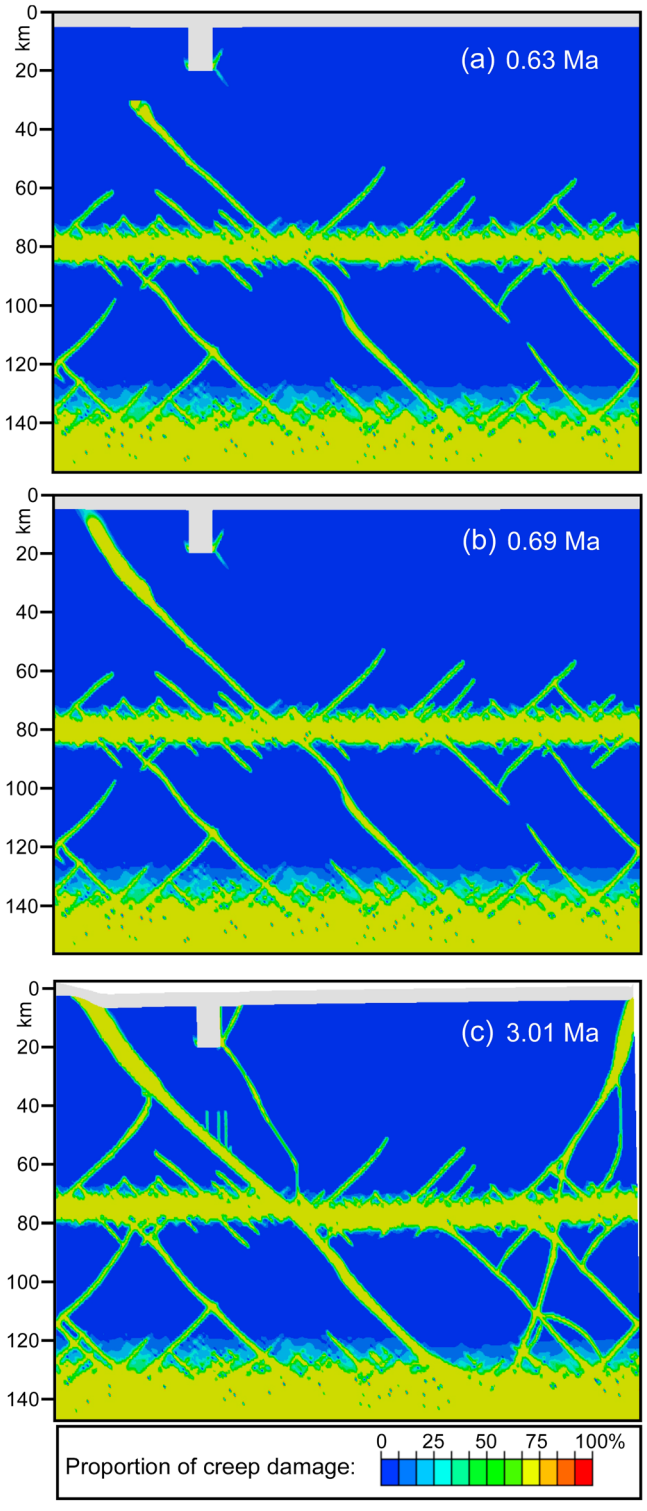

Figure 5. Evolution of brittle and creep damage in the same model shown in Figure 4, with a subcritical notch depth of 20 km, an asymmetric extension velocity, and a mantle heat flow of 30 mW/m^2.

3. Results

3.1. Models With a Subcritical Notch Depth

We first discuss model results without a notch [*Liu et al.*, 2014], which are equivalent to models where the depth of the notch is shallower than the critical depth of 20 km (Figure 4) and show a similar behavior. At the very early stages (<55 kyr) of extension, no localized damage is observed in the brittle crust. However, the ductile part of the lithosphere features a very rich dynamics, illustrated by the pattern of creep and melt damage bands (Figure 4a). Conjugate pairs of high-porosity damage bands form as a result of creep fractures at shallower depth (Figure 4a), whereas partial melting occurs at the bottom of the lithosphere (Figure 4b). Surprisingly, these two subhorizontal damage bands require only a small input of mechanical work, which is supplied by the slow extension over ~50 kyr. This small input of mechanical work suffices to change the thermodynamic conditions such that melting is possible at the base of a low surface heat flow lithosphere (Figure 4b), communicating with an equivalent metamorphic fluid driven creep fracture layer at shallower depths (Figure 4a). As noted earlier, the exact depth of these layers is controlled by the geothermal conditions. In other words, the melting layer will be shallower and thicker in models with the same surface heat flow but higher mantle heat flows. This effectively results in pushing the creep and melt damage layers closer to the surface.

The model shown in Figure 4 is just below the point of critical notch depth for the given boundary conditions. It has a notch depth of 20 km, an asymmetric extension velocity, a higher mantle heat flow of 30 mW/m^2, and a surface heat flow of 50 mW/m^2. After 55 kyr damage in the molten layer at the base of the model propagates upward, whereas damage in the creep section of the upper mantle propagates both upward and downward, forming a damage band that connects the two layers (Figure 4a). Note that this interaction results in a slight bending of the damage/high-porosity band. The middle damaged layer has no melt (Figure 4b) and is in the viscous

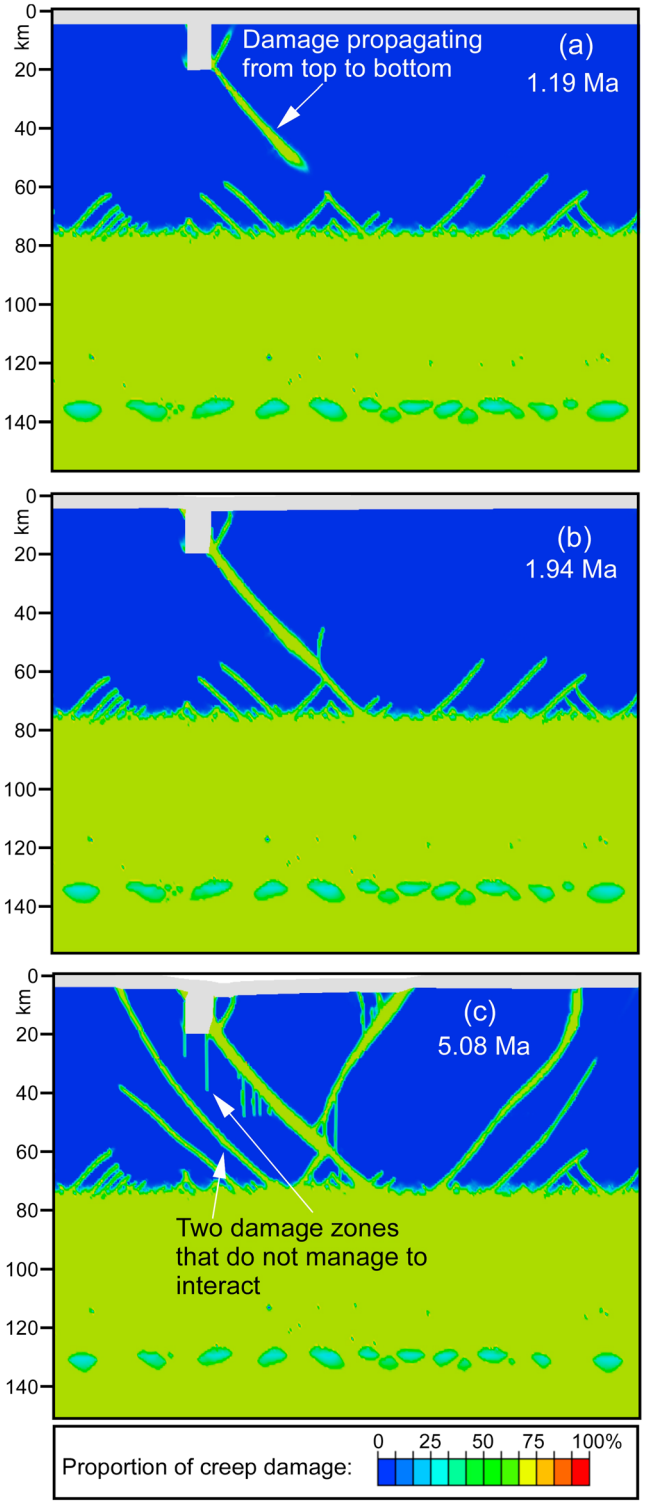

Figure 6. Evolution of the brittle and creep damage of a model with symmetric extension velocity and a lower mantle heat flow of 20 mW/m^2. A deeper notch depth of 20 km turns into a supercritical notch. (a) 1.19 Ma, (b) 1.94 Ma, and (c) 5.08 Ma.

domain. Therefore, the dominant instability is associated with the ductile damage mechanism. The lower damaged layer has melt (Figure 4b), which decreases its strength and allows for earlier development of creep damage (see creep damage assisted by melt in Figure 4a). The middle creep damage layer is located just above the zone of partial melting. We attribute this to the strength amplification above the fast creeping melt-damaged layer. The transition between the melt damaged zone and the area without melt damage results in stress concentration leading to the nucleation of localized creep.

The evolution of damage through time in the same model (Figure 5) shows that the creep damage propagates upward to the surface. It initially only reaches the Moho (Figure 5a), but then propagates rapidly through the crust. Note that up to this point, the notch does not play any role in this model, and the results are essentially similar to those obtained in models without a notch [*Liu et al.*, 2014].

Figure 5b shows a later stage of the evolution when the first damage zone crosses the entire crust and reaches the surface. This zone is not affected by the preexisting notch, and its location is defined by the processes in the deep layers. The structure is stable and preserved for relatively long time. Only after ~3 Ma (Figure 5c), brittle damage emerges from the edge of the notch and propagates downward, linking the notch with the creep-damage layer. However, the original damage zone away from the notch still remains dominant and is expected to be the main path for the melt to propagate from the asthenosphere into the lithosphere and to the surface.

3.2. Models With a Supercritical Notch Depth

The difference between the models with or without a notch only becomes apparent when the notch reaches a critical depth of 20 km. A subtle

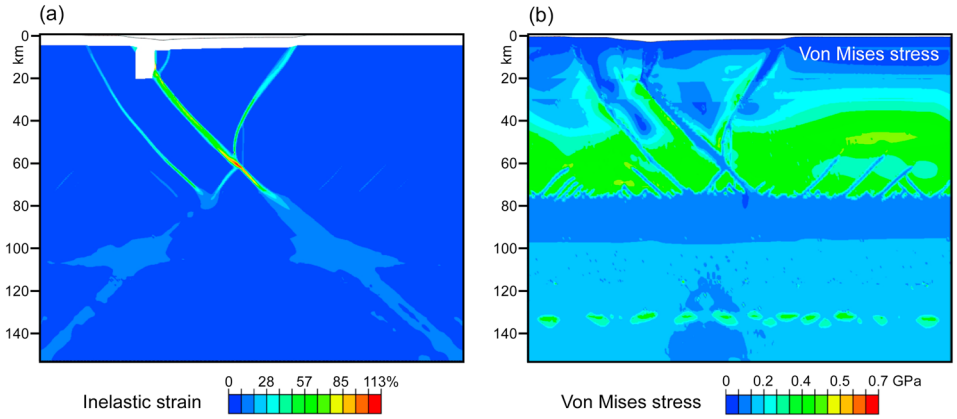

Figure 7. Results of a supercritical model (same parameters as Figure 6) at $t = 3.64$ Ma. (a) Inelastic strain and (b) von Mises shear stress.

difference in the various model runs is observed in the dynamics of the linkage between the creep and melt damage zones. However, the most substantial difference is observed when the two deep damage mechanisms ultimately interact with the brittle damage as described in the following section. Both the symmetric velocity boundary conditions and the lower mantle heat flow lead to an earlier transition from subcritical to critical notch depth.

Results of a symmetric model with a similar 20 km depth notch and a lower value of mantle heat flow (20 mW/m^2) are presented in Figures 6 and 7. Here the existence of the notch becomes critical. The effect of the symmetric extension is that it enhances deformation at the top, thus deemphasizing deeper processes. Also, because it has a lower mantle temperature, the melt layer is much thinner leading to less creep and melt damage, thereby decreasing weakening at depth. Therefore, the dominant damage zone is nucleated at the bottom edge of the notch and propagates downward (Figure 6a). This single damage zone connects the notch with the creep damage layer and remains dominant during a long period (~2 Ma; Figure 6b). At a later stage (~5 Ma), additional subparallel and conjugate features are formed (Figure 6c). Most of the inelastic deformation is accommodated by two zones; one associated with the notch and another zone in a conjugate direction (Figure 7a). Most of the surface subsidence occurs between these zones. Influencing the criticality of the model by second-order effects, such as using low mantle heat flow and symmetric extension, leads to less prominent localization around the notch. A more efficient way to localize deformation around the notch is by simply increasing the notch depth.

The critical role of the notch depth is illustrated in the results of a model that has a slightly deeper notch of 20.4 km (Figure 8). The mantle heat flow in this model is 25 mW/m^2 and the surface heat flow remained at 50 mW/m^2. The results show that the effect of a notch with only 0.4 km greater depth is significant. The notch strongly attracts two subparallel upward propagating shear zones that are focused on the two corners of the notch (Figure 8a). This leads to the formation of another conjugate set of shear zones propagating to the right of the notch (Figure 8b). The resulting configuration allows a single channel of significant width to connect the partially molten layer with the surface, with a preference to the proximity of the notch. Furthermore, the model creates a single deep triangular trough (right of the notch in Figure 8b), which could potentially trap the melt, thus forming a volcanic field in a deep depression.

4. Discussion

4.1. The Role of Damage Mechanics in Melt Generation

Our results show that a lithosphere subjected to slow extension can melt at its base owing to a small input of mechanical work dissipated by the deformation. The melt fraction is expected to initially be low, but it can be enhanced by the choice of an asymmetric extension velocity with higher velocities at the bottom of the lithosphere. This early formation of melt damage interacts with creep fractures that are present at shallower

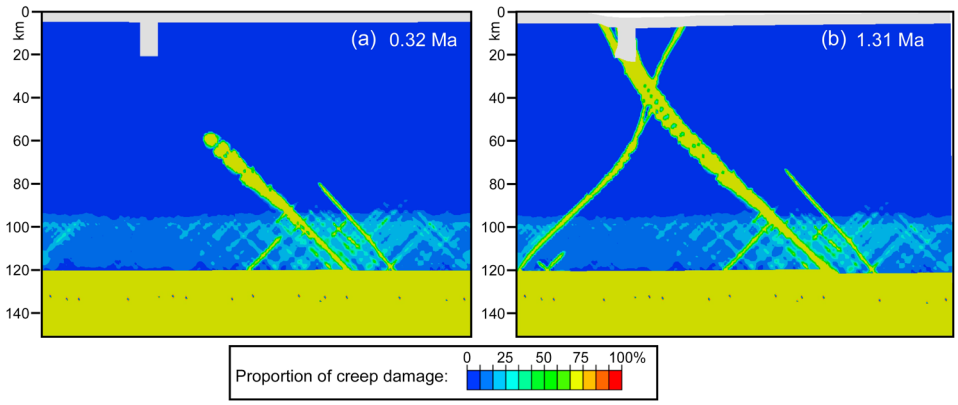

Figure 8. Evolution of the brittle and creep damage for a supercritical model with a symmetric extension, a notch depth of 20.4 km, and a mantle heat flow of 25 mW/m^2. (a) 0.32 Ma and (b) 1.31 Ma.

level, leading to further focusing of mechanical work in the partially molten layer, and positive feedback through additional melting.

The rate of creep damage mechanisms is controlled by metamorphic reactions accommodating the applied strain. Such chemically controlled plastic strain is a result of dissolution of matter and reprecipitation in places that accommodate the strain. As there are a number of other more efficient deformation mechanisms available at higher stress and deformation rates (e.g., dislocation creep, dislocation glide, and brittle fracture), this type of chemically facilitated creep is typically attributed to the group of (low stress-low strain rate) chemical diffusion end-member creep mechanisms [*Ashby and Verall*, 1977]. These low strain rate processes can be very efficient if a small amount (e.g., 1%) of hydrous fluid is available [*Menegon et al.*, 2008]. Therefore, the choice of a very low extension velocity in our models suppressed brittle deformation and favored creep and melt damage mechanisms. In simple terms, this implies that models with low velocities are dominated by creep localization mechanisms, which means that shear zones evolve from the bottom up.

For a fast extension velocity, creep localization mechanisms are suppressed [*Karrech et al.*, 2011a] and the lower part of the model deforms homogeneously with limited formation of melt channels. Therefore, an important conclusion of this study is that low extension velocities are critical for the formation of intraplate volcanism. As both creep and melt damage mechanisms are facilitated by growth of fluid-filled voids through a creep mechanism, a slower extension velocity leads, counterintuitively, to more efficient localization.

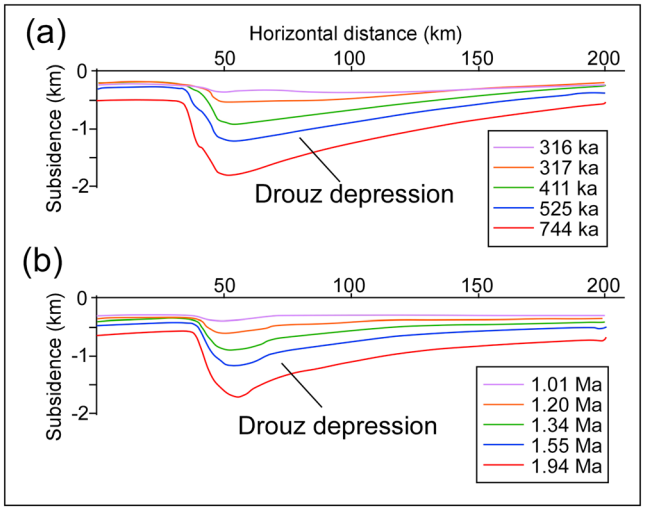

Figure 9. Subsidence curves for the two models with a supercritical notch. (a) Symmetric extension with a notch depth of 20.4 km and a mantle heat flow of 25 mW/m^2 (see Figure 8). (b) Symmetric extension with a notch depth of 20 km and a mantle heat flow of 20 mW/m^2 (see Figures 6 and 7).

Another feature of the low extension velocity is that shear heating is extremely low and is everywhere less than 7°C. It is interesting that in spite of the low shear heating, the width of the shear zone and the damage are still entirely controlled by the thermal solution. When there is no geometric interaction with boundaries or other shear zones, the width of shear zones corresponds to the thermal diffusion length scale (see Figures 3 and 5 in *Karrech et al.* [2011a]).

4.2. Subsidence and Comparison to the Azraq-Sirhan

Models with supercritical notch depths resulted in a similar asymmetric surface subsidence, with the surface notch acting as an attractor to the deep deformation. A comparison of the surface depression for the two aforementioned critical models (Figure 9) shows a distinct asymmetric depression of 1–2 km with a characteristic wavelength of ~200 km. The results are calculated for the reference extension velocity of 1 mm/yr and indicate how much time it takes to form the surface depression.

The comparable geological evidence for surface depression in the proximity of the Azraq-Sirhan Graben is the Drouz Depression (Figure 1c), which was first filled with Tertiary sediments and subsequently filled with basalt. Based on our numerical models, we interpret that the time lag between sedimentary and magmatic infill is associated with the time taken for the brittle and ductile damage zone to fully interact with melt damage from below. This time lag is significantly longer for the model with a 20 km notch and mantle heat flow of 20 mW/m^2 (Figures 6, 7, and 9b) in comparison with the model that has a 20.4 km notch and mantle heat flow of 25 mW/m^2 (Figures 8 and 9a). This is because before connecting to the melt-bearing (melt-rich) bands deep in the lithosphere, the brittle and ductile damage network in the overlying melt-free layers need to mature significantly. As the approximate thickness of the Tertiary sedimentary infill equates to about 1 km (see Figure 1c), a significant time lapse for transition from sedimentary infill to magmatic infill is required. We therefore argue that models such as the one shown in Figures 6 and 7 provide a better representation of the possible time evolution.

A striking result is that in both models with a supercritical notch, a 2 km deep graben is established in a few million years. We have chosen in our example a relatively slow velocity of 1 mm/yr, which leads to strong weakening and discrete jumps in topography within the 200 km wavelength. Using existing geological data from the Azraq-Sirhan Graben [*Konert et al*., 2001, Figure 1], we cannot resolve the detailed topography of the graben and cannot derive the subsidence rates and extension velocity. We argue that the fast subsidence in our model probably overestimates the required extension rate.

We speculate that both the deep notch model (Figure 8) and the critical notch model (Figures 6 and 7) can explain the principal observations of the Azraq-Sirhan magmatic activity. Both models feature a transition from magma absent to magma-rich extension. Furthermore, both models show that damage is localized in the proximity of the preexisting defect (Azraq-Sirhan Graben) and leads to an asymmetric triangular depression (Drouz Depression). This depression is filled with the melt likely to have been produced in the localized shear zones, thus explaining the occurrence of the Harrat Ash-Shaam volcanic field.

4.3. Time Lag, Breakthrough of Magma, and Limit of Model Validity

The expected time lag between the onset of basin subsidence and the arrival of magma to the surface, related to the breakthrough of melt-conduit shear zones at the surface, is a robust model prediction that could be tested against natural examples. Calculations are reasonably accurate until this point. Although we do not calculate melt transfer explicitly, we expect a relatively little melt transfer through the shear zones until they breach the surface. After breaching the surface, the models become less accurate because they do not include melt transfer and related heat advection. When they do breach the surface, we expect that shear zones become important melt conduits capable of transferring significant volumes of melt. In the case of the Harrat Ash-Shaam volcanic field, kilometer-thick lava flows have ponded in the Drouz depression (Figure 1c). Such voluminous melt transfer would have significantly changed the distribution of heat in the system. Since melt transfer is not included, the models are only useful for assessing preeruption scenarios, or possibly some posteruption scenarios, such as the European intraplate province, where only minor amounts of melt have reached the surface. The validity of the thermal model prediction following onset of volcanism therefore becomes a case by case study and loses its generality. The time lag in this contribution is therefore only illustrated in the kinematic field through the comparison between the vertical motion and the damage evolution. It follows that for different kinematic boundary conditions, the time lag is inversely proportional to the change in extension velocity. For a lower extension velocity, the lag increases while for a faster velocity it decreases proportionally.

5. Conclusions

Multiple feedback mechanisms active in the accommodation of strain in the presence of fluids are capable of generating melts in the lithosphere/asthenosphere in regions of relatively low heat flux. This then generates

high-porosity lithospheric-scale shear zones capable of transferring melts and fluids to the surface. Efficient localization in the weaker ductile domains imply that the final pattern of strain distribution is controlled from below rather than above, explaining why in some cases the notch in the upper crust is bypassed by the lithospheric shear zones. When the notch is sufficiently deep, it partly controls the location of the shear zones and consequently also the magma transfer to the surface.

The model provides an explanation for intraplate volcanism in slowly deformed lithospheres, highlighting the transition from magma-absent to magma-present extension. A significant finding is that slow extension, rather than fast extension, can localize melt damage more effectively in the deep lithosphere. Another important model prediction is that we expect a considerable lag between the formation of surface tectonic features and the onset of volcanism. These findings may have profound implications to the fundamental dynamic control on intraplate volcanism.

Acknowledgments

The development of the basic theory for this research was funded by the Australian Research Council (grant DP1094050) and a UQ-UWA collaboration award. K.R.L. and J.L. would like to acknowledge support by the University of Western Australia and CSIRO. A.S. and V.L. acknowledge support by the Israel Science Foundation (ISF 753/08). The results can be reproduced using the references provided. The formulation itself is published in *Liu et al*. [2014], and the geological material is accessible from the provided literature.

References

ABAQUS/Standard (2000), *Hibbit*, pp. 384, Karlsson and Sorenson Inc., Pawtucket, R. I.

Anderson, D. L., Y.-S. Zhang, and T. Tanimoto (1992), Plume heads, continental lithosphere, flood basalts and tomography, in *Magmatism and the Causes of Continental Break-up*, edited by B. C. Storey, T. Alabaster, and R. J. Pankhurst, pp. 99–124, Geological Society, London.

Ashby, M. F., and R. A. Verall (1977), Micromechanisms of flow and fracture, and their relevance to the rheology of the upper mantle, *Philos. Trans. R. Soc. London*, *288*, 59–95.

Avni, Y., A. Segev, and H. Ginat (2012), Oligocene regional denudation of the northern Afar dome: Pre- and syn-breakup stages of the Afro-Arabian Plate, *Geol. Soc. Am. Bull.*, *124*, 1871–1897, doi:10.1130/B30634.1.

Buck, W. R. (2006), The role of magma in the development of the Afro-Arabian Rift System, in *The Afar Volcanic Province Within the East African Rift System*, edited by G. Yirgu, C. J. Ebinger, and P. K. H. Maguire, *Geol. Soc. London Spec. Publ.*., *259*, 43–54.

Camp, V. E., M. J. Roobol, and P. R. Hooper (1992), The Arabian continental alkali basalt province, Part 3: Evolution of Harrat Kishb, Kingdom of Saudi Arabia, *Geol. Soc. Am. Bull.*, *104*, 379–396.

Chrysochoos, A., and F. Belmahjoub (1992), Thermographic analysis of thermomechanical couplings, *Arch. Mech.*, *44*(1), 55–68.

Conrad, C. P., T. A. Bianco, E. I. Smith, and P. Wessel (2011), Patterns of intraplate volcanism controlled by asthenospheric shear, *Nat. Geosci.*, *4*(5), 317–321.

Downes, H. (1990), Shear zones in the upper mantle—Relations between geochemical enrichment and deformation in mantle peridotites, *Geology*, *18*, 374–377.

Eichhubl, P., and A. Aydin (2002), Ductile opening-mode fracture by pore growth and coalescence during combustion alteration of siliceous mudstone, *J. Struct. Geol.*, *25*(1), 121–134.

Eldholm, O., and K. Grue (1994), North Atlantic volcanic margins: Dimensions and production rates, *J. Geophys. Res.*, *99*(B2), 2955–2968, doi:10.1029/93JB02879.

Fliertvoet, T., S. C. White, and M. R. Drury (1997), Evidence for dominant grain boundary sliding in greenschist and amphibolite facies conditions from the Redbank Deformed Zone, Central Australia, *J. Struct. Geol.*, *19*(12), 1495–1520.

Förster, A., H.-J. Förster, R. Masarweh, A. Masri, K. Tarawneh, and DESERT Group (2007), The surface heat flow of the Arabian Shield in Jordan, *J. Asian Earth Sci.*, *30*, 271–284.

Förster, H.-J., A. Förster, R. Oberhänsli, and D. Stromeyer (2010), Lithospheric composition and thermal structure of the Arabian Shield in Jordan, *Tectonophysics*, *481*, 29–37.

Fusseis, F., K. Regenauer-Lieb, J. Liu, R. M. Hough, and F. De Carlo (2009), Creep cavitation can establish a dynamic granular fluid pump in ductile shear zones, *Nature*, *459*(7249), 974–977.

Garfunkel, Z. (1989), Tectonic setting of Phanerozoic magmatism in Israel, *Isr. J. Earth Sci.*, *38*, 51–74.

Ghandi, C., and M. F. Ashby (1979), Overview No. 5: Fracture-mechanism maps for materials which cleave: F.C.C., B.C.C. and H.C.P. metals and ceramics, *Acta Metall.*, *27*, 1565–1602.

Holtzman, B. K., D. S. H. King, and D. L. Kohlstedt (2012), Effects of stress-driven melt segregation on the viscosity of rocks, *Earth Planet. Sci. Lett.*, *359–360*, 184–193, doi:10.1016/j.epsl.2012.09.030.

Houlsby, G., and A. Puzrin (2007), *Principles of Hyperplasticity: An Approach to Plasticity Theory Based on Thermodynamic Principles*, 351 pp., Springer, Berlin.

Karrech, A., K. Regenauer-Lieb, and T. Poulet (2011a), Continuum damage mechanics for the lithosphere, *J. Geophys. Res.*, *116*, B04205, doi:10.1029/2010JB007501.

Karrech, A., K. Regenauer-Lieb, and T. Poulet (2011b), A damaged visco-plasticity model for pressure and temperature sensitive geomaterials, *J. Eng. Sci.*, *49*, 1141–1150.

Konert, G., A. M. Afifi, S. A. Al-Harjri, and H. J. Droste (2001), Paleozoic stratigraphic and hydrocarbon habitat of the Arabian Plate, *GeoArabia*, *6*, 407–442.

Liu, J., A. Karrech, and K. Regenauer-Lieb (2014), Combined mechanical and melting damage model for geomaterials, *Geophys. J. Int.*, *198*(3), 1319–1328, doi:10.1093/gji/ggu200.

Lyakhovsky, V., A. Segev, U. Schattner, and R. Weinberger (2012), Deformation and seismicity associated with continental rift zones propagating toward continental margins, *Geochem. Geophys. Geosyst.*, *13*, Q01012, doi:10.1029/2011GC003927.

Ma, G. S.-K., J. Malpas, C. Xenophontos, and G. H.-N. Chan (2011), Petrogenesis of latest Miocene-Quaternary continental intraplate volcanism along the Northern Dead Sea Fault System (Al Ghab–Homs Volcanic Field), Western Syria: Evidence for lithosphere-asthenosphere interaction, *J. Petrol.*, *52*(2), 401–430, doi:10.1093/petrology/egq085.

McKenzie, D., and M. J. Bickle (1988), The volume and composition of melt generated by extension of the lithosphere, *J. Petrol.*, *26*, 625–679.

McKenzie, D., and R. K. O'Nions (1991), Partial melt distributions from inversion of rare-Earth element concentrations, *J. Petrol.*, *32*(5), 1021–1091.

Meiler, M., M. Reshef, and H. Shulman (2011), Seismic depth-domain stratigraphic classification of the Golan Heights, central Dead Sea Fault, *Tectonophysics*, *510*(3–4), 354–369, doi:10.1016/j.tecto.2011.08.007.

Menegon, L., G. Pennacchioni, and R. Spiess (2008), Dissolution-precipitation creep of K-feldspar in mid-crustal granite mylonites, *J. Struct. Geol.*, *30*(5), 565–579, doi:10.1016/j.jsg.2008.02.001.

Nocquet, J. M., E. Calais, Z. Altamimi, P. Sillard, and C. Boucher (2001), Intraplate deformation in western Europe deduced from an analysis of the International Terrestrial Reference Frame 1997 (ITRF97) velocity field, *J. Geophys. Res.*, *106*(B6), 11,239–11,257, doi:10.1029/2000JB900410.

Poulet, T., E. Veveakis, K. Regenauer-Lieb, and D. Yuen (2014), Thermo-poro-mechanics of chemically active creeping faults. 3: The role of serpentinite in episodic tremor and slip sequences, and transition to chaos, *J. Geophys. Res. Solid Earth*, *119*, 4606–4625, doi:10.1002/2014JB011004.

Raj, R. (1982), Creep in polycrystalline aggregates by matter transport through a liquid phase, *J. Geophys. Res.*, *87*(B6), 4731–4739, doi:10.1029/JB087iB06p04731.

Razvalyaev, A. V., V. G. Kazmin, and A. B. Galaktionov (2005), Volcanism, in *Geological Framework of the Levant, Cyprus and Syria*, vol. 1, edited by V. A. Krasheninnikov et al., pp. 417–462, Historical Productions-Hall, Jerusalem.

Regenauer-Lieb, K. (1999), Dilatant plasticity applied to Alpine collision: ductile void growth in the intraplate area beneath the Eifel volcanic field, *J. Geodyn.*, *27*(1), 1–21, doi:10.1016/S0264-3707(97)00024-0.

Regenauer-Lieb, K., and J. P. Petit (1997), Cutting of the European continental lithosphere: Plasticity theory applied to the present Alpine collision, *J. Geophys. Res.*, *102*(B4), 7731–7746, doi:10.1029/96JB03409.

Regenauer-Lieb, K., and D. A. Yuen (2003), Modeling shear zones in geological and planetary sciences: Solid- and fluid-thermal-mechanical approaches, *Earth Sci. Rev.*, *63*, 295–349.

Regenauer-Lieb, K., R. F. Weinberg, and G. Rosenbaum (2006), The effect of energy feedbacks on continental strength, *Nature*, *442*, 67–70.

Regenauer-Lieb, K., et al. (2013a), Multiscale coupling and multiphysics approaches in Earth science: Applications, *J. Coupled Syst. Multiscale Dyn.*, *1*(3), 281–323, doi:10.1166/jcsmd.2013.1021.

Regenauer-Lieb, K., M. Veveakis, T. Poulet, F. Wellmann, A. Karrech, J. Liu, J. Hauser, C. Schrank, O. Gaede, and M. Trefry (2013b), Multiscale coupling and multiphysics approaches in Earth sciences: Theory, *J. Coupled Syst. Multiscale Dyn.*, *1*(1), 49–73, doi:10.1166/jcsmd.2013.1012.

Rosenbaum, G., K. Regenauer-Lieb, and R. F. Weinberg (2010), Interaction between mantle and crustal detachments: A non-linear system controlling basin formation, *J. Geophys. Res.*, *115*, B11412, doi:10.1029/2009JB006696.

Rybacki, E., R. Wirth, and G. Dresen (2008), High-strain creep of feldspar rocks: Implications for cavitation and ductile failure in the lower crust, *Geophys. Res. Lett.*, *35*, L04304, doi:10.1029/2007GL032478.

Rybacki, E., R. Wirth, and G. Dresen (2010), Superplasticity and ductile fracture of synthetic feldspar deformed to large strain, *J. Geophys. Res.*, *115*, B08209, doi:10.1029/2009JB007203.

Schattner, U., Z. Ben-Avraham, M. Lazar, and C. Hüebscher (2006), Tectonic isolation of the Levant basin offshore Galilee-Lebanon—Effects of the Dead Sea fault plate boundary on the Levant continental margin, eastern Mediterranean, *J. Struct. Geol.*, *28*(11), 2049–2066, doi:10.1016/j.jsg.2006.06.003.

Segev, A., and M. Rybakov (2010), Effects of Cretaceous plume and convergence, and Early Tertiary tectonomagmatic quiescence on the central and southern Levant continental margin, *J. Geol. Soc.*, *167*(4), 731–749, doi:10.1144/0016-76492009-118.

Segev, A., and M. Rybakov (2011), History of faulting and magmatism in the Galilee (Israel) and across the Levant continental margin inferred from potential field data, *J. Geodyn.*, *51*(4), 264–284, doi:10.1016/j.jog.2010.10.001.

Segev, A., U. Schattner, and V. Lyakhovsky (2011), Middle-late Eocene structure of the southern Levant continental margin—Tectonic motion versus global sea-level change, *Tectonophysics*, *499*(1–4), 165–177, doi:10.1016/j.tecto.2011.01.006.

Segev, A., V. Lyakhovsky, and R. Weinberger (2014), Continental transform-rift interaction adjacent to a continental margin: The Levant case study, *Earth Sci. Rev.*, *193*, 83–103.

Shalev, E., V. Lyakhovsky, Y. Weinstein, and Z. Ben-Avraham (2013), The thermal structure of Israel and the Dead Sea Fault, *Tectonophysics*, *602*, 69–77, doi:10.1016/j.tecto.2012.09.011.

Sharland, P. R., R. Archer, D. M. Casey, R. B. Davies, S. H. Hall, A. P. Heward, A. D. Horbury, and M. D. Simmons (2001), *Arabian Plate Sequence Stratigraphy*, *GeoArabia Spec. Publ.*, vol. 2, 371 pp., Gulf PetroLink, Bahrain.

Sibson, R. H. (1985), A note on fault reactivation, *J. Struct. Geol.*, *7*(6), 751–754.

Steckler, M. S., and U. S. ten Brink (1986), Lithospheric strength variations as a control on new plate boundaries: Examples from the northern Red Sea region, *Earth Planet. Sci. Lett.*, *79*(1–2), 120–132, doi:10.1016/0012-821X(86)90045-2.

Turcotte, D. L., and G. Schubert (2002), *Geodynamics*, 456 pp., Cambridge Univ. Press, New York.

Veveakis, M., and T. Poulet (2014), Thermo-poro-mechanics of chemically active creeping faults: 2. Transient considerations, *J. Geophys. Res. Solid Earth*, *119*, 4583–4605, doi:10.1002/2013JB010071.

Weinberg, R. F., and K. Regenauer-Lieb (2010), Ductile fractures and magma migration from source, *Geology*, *38*(4), 363–366.

Weinstein, Y., O. Navon, R. Altherr, and M. Stein (2006), The Role of lithospheric mantle heterogeneity in the generation of Plio-Pleistocene alkali basaltic suites from NW Harrat Ash-Shaam (Israel), *J. Petrol.*, *47*(5), 1017–1050, doi:10.1093/petrology/egl003.

Willan, R. C. R., and S. P. Kelley (1999), Mafic dike swarms in the South Shetland Islands volcanic arc: Unravelling multiepisodic magmatism related to subduction and continental rifting, *J. Geophys. Res.*, *104*(B10), 23,051–23,068, doi:10.1029/1999JB900180.

Wilson, M., and H. Downes (1992), Mafic alkaline magmatism associated with the European Cenozoic rift system, *Tectonophysics*, *208*, 173–182.